

DPSK/FSK Hybrid Modulation Format and Analysis of Its Nonlinear Performance

Fangfei Liu, *Student Member, IEEE*, and Yikai Su, *Senior Member, IEEE*

Abstract—We propose a novel hybrid modulation format—differential phase shift keying with frequency shift keying labeling for optical label switching. A modulation technique based on a dual-parallel Mach–Zehnder modulator and a label erasing scheme are presented. The tolerance of the new format to intrachannel four-wave mixing at high speeds is studied analytically and through simulations, which show robustness to nonlinear impairments.

Index Terms—Nonlinear distortion, optical Kerr effect, phase modulation, photonic switching systems.

I. INTRODUCTION

OPTICAL label switching is a promising technology for future all-optical packet-rate routing and forwarding [1]–[3]. Hybrid modulation techniques allow adding and removing label information on the payload packets. Some hybrid formats have been proposed and experimentally demonstrated, such as amplitude shift keying (ASK) with differential phase shift keying (DPSK) labeling (ASK/DPSK) [4]–[7], DPSK with ASK labeling (DPSK/ASK) [8]–[11], and intensity modulation with frequency shift keying (IM/FSK) [12], [13]. The use of the DPSK for long-haul transmission instead of the on–off keying (OOK) is primarily due to the higher receiver sensitivity using balanced detection and its better nonlinear performance, which is partly attributed to the lower peak power of the DPSK signals [14]. In ultra long-haul pseudolinear transmission systems, intrachannel cross-phase modulation (IXPM) and intrachannel four-wave mixing (IFWM) are the major nonlinear degradation factors [15]. Although the IXPM can be almost suppressed by using a symmetric dispersion map [16], the IFWM remains a challenge. The DPSK was shown to be effective in suppressing the IFWM to a certain extent in highly nonlinear transmission regimes because of the lower peak power and partial cancellation of the nonlinear phase shifts [14]. The FSK format, like the DPSK, possesses constant energy per bit and improved receiver sensitivity if equipped with balanced detection. Therefore, it is of interest to explore the performance of a hybrid modulation format using DPSK as the payload and FSK as the label. As this hybrid format also shows constant energy in all bit slots,

penalties that are associated with the intensity modulation that results in poor extinction ratio, as seen in all the previous hybrid formats [4]–[13] employing intensity modulation, are eliminated. Furthermore, as the FSK can be viewed as a special phase modulation format imposing a variable phase on top of the DPSK signal, our hybrid format may improve the nonlinear properties by reducing the imaginary part of the IFWM components that affect the signal phase [17]. Prior to this paper, the combination of the DPSK and the FSK has not yet been proposed and studied primarily due to unavailable device technology for the generation and demodulation of the format.

However, the proposed format is feasible, as shown by recent works on modulation techniques and the demonstrated devices. In [18] and [19], a dual-parallel modulator has been proposed. We find that this modulator can be also used to simultaneously generate DPSK and FSK formats. At a receiving site, label erasing can be achieved by employing a double sideband (DSB) modulator based on a standard Mach–Zehnder modulator (MZM) [12], [20], [21]. After the erasure of the FSK signal, the DPSK signal is detected using a one-bit delay Mach–Zehnder interferometer (MZI).

We study the IFWM effects in the hybrid DPSK/FSK modulation format by theoretical analysis and numerical simulations. A previous IFWM analysis of a pseudolinear subchannel multiplexed system was presented in [22], which shows certain similarities with ASK/FSK and DPSK/FSK systems. In this paper, the performance degradation due to the IFWM of the hybrid DPSK/FSK format is investigated in detail. We find that, in addition to the fact that the IFWM-induced amplitude fluctuation exponentially decreases with the increasing of the frequency space as addressed in [22], the IFWM component of the DPSK/FSK signal presents a special frequency deviation that is different from that of the pulse where the IFWM component is located. The above properties of the IFWM process associated with the DPSK/FSK format imply that the nonlinear transmission performance of the new format improves upon the modulation of the label information, making it attractive for long-haul high-speed labeled transmission. We also discuss the dispersion slope tolerance of this hybrid modulation format. We note that the improved nonlinear performance of the format comes with the decreased spectral efficiency because of the wider bandwidth of the signal; therefore, balance between the nonlinear transmission performance and the spectral efficiency is needed depending on the application scenarios.

In Section II-A, we introduce the signal generation scheme, and in Section II-B, we describe label erasing and the detection of the label and the payload. We study the effect of the IFWM on the DPSK/FSK format in Section III, and the dispersion slope tolerance of the DPSK/FSK is discussed in Section IV.

Manuscript received February 28, 2007; revised July 29, 2007. This work was supported by the National Natural Science Foundation of China (60407008), the 863 High-Tech program (2006AA01Z255), the key project of Ministry of Education (106071), and the Fok Ying Tung Fund (101067).

The authors are with State Key Laboratory of Advanced Optical Communication Systems and Networks, Department of Electronic Engineering, Shanghai Jiao Tong University, Shanghai 200240, China (e-mail: yikaisu@sjtu.edu.cn).

Color versions of one or more of the figures in this paper are available online at <http://ieeexplore.ieee.org>.

Digital Object Identifier 10.1109/JLT.2007.909906

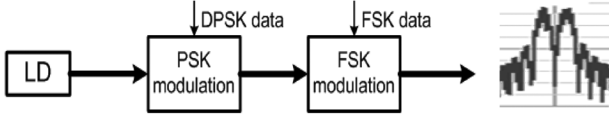


Fig. 1. General modulation scheme and the spectrum of the DPSK/FSK signal.

II. SIGNAL GENERATION AND DETECTION

A. Modulation Principle

In general, the generation of the DPSK/FSK consists of two phases of modulations (Fig. 1)—one is the generation of the optical DPSK packet signal, and the other is to add the label information. When the label information is “1,” the carrier frequency of the optical DPSK signal is $f_0 + f_m$, whereas if the label information is “0,” the carrier frequency becomes $f_0 - f_m$, where f_0 and f_m are the original carrier frequency and the frequency deviation, respectively. It should be mentioned that, for simplicity, we use “carrier” to stand for the central frequency of the DPSK signal, although it does not show a discrete tone. For the generation of the hybrid DPSK/FSK modulation format, one crucial concern is to ensure that the carriers at frequency $f_0 + f_m$ and $f_0 - f_m$ have consistent initial phases so as not to affect the phase of the DPSK signal.

Here, we propose the use of a dual-parallel modulator (Fig. 2), which can induce varied phases denoted by $\varphi_{A1}, \varphi_{A2}, \varphi_{B1}, \varphi_{B2}, \varphi_{C1}$, and φ_{C2} [18] on the six arms to simultaneously implement DPSK and FSK modulations. The initial phases of the two carriers can be kept consistent by properly driving the six phase modulators, which would be impossible with x-cut dual-parallel modulators.

The modulator is mainly configured as an FSK modulator. When there is no DPSK modulation, the two sub-MZMs operate in push-pull configuration, and they are biased at null points. Two cosine signals with a frequency of f_m and a phase difference of 180° expressed as $A_m \cos \omega_m t$ ($\omega_m = 2\pi f_m$) and $A_m \cos(\omega_m t + \pi)$ are applied to the upper sub-MZM, whereas two sine signals with the same frequency of f_m and opposite phases denoted as $A_m \sin \omega_m t$ and $A_m \sin(\omega_m t + \pi)$ are added to the lower sub-MZM. φ_{C1} is kept to be 0° , and φ_{C2} is controlled by the FSK data. When the FSK driving signal is $V_\pi/2$, where V_π is the switching voltage, i.e., $\varphi_{C2} = +\pi/2$, the upper sideband (USB) signal at $f_0 + f_m$ is achieved. On the other hand, if the FSK signal is $-V_\pi/2$ and, correspondingly, $\varphi_{C2} = -\pi/2$, the lower sideband (LSB) signal at $f_0 - f_m$ with the same initial phase as that of the USB is generated [19]. If φ_{C2} is expressed as $f(t) = \pm\pi/2$, the output of the modulator can be written as [23]

$$\begin{aligned} E_c &= E_a + \exp[i f(t)] E_b \\ &= \frac{1}{2} \exp\left[i\left(\omega_0 t + \frac{\pi}{2}\right)\right] J_1(A_m) \\ &\quad \times (\{1 + \sin[f(t)]\} \exp(i\omega_m t) \\ &\quad + \{1 - \sin[f(t)]\} \exp(-i\omega_m t)) \end{aligned} \quad (1)$$

where E_a and E_b are the outputs of the two sub-MZMs, and J_1 is the coefficient of the first-kind first-order Bessel function.

Once the FSK data are generated, the precoded DPSK signal $\text{data}(t)$ is superimposed to each of the four clock signals, where $\text{data}(t) = 0$ or V_π ; the four paths of the sub-MZMs experience the same additional phase shift that is determined by the DPSK signal. This “common-mode” operation is equivalent to driving a phase modulator on top of the FSK modulation. Thus, it achieves the same function as sending a DPSK signal into an FSK modulator, as sketched in Fig. 1. Therefore, the outputs of the two sub-MZMs become $\exp[i\pi \times \text{data}(t)/V_\pi] E_a$ and $\exp[i\pi \times \text{data}(t)/V_\pi] E_b$, respectively. The common factor $\exp[i\pi \times \text{data}(t)/V_\pi]$ can be extracted out; therefore, the output of the modulator becomes

$$\begin{aligned} E'_c &= \exp\left[i\frac{\pi}{V_\pi} \text{data}(t)\right] \{E_a + \exp[i f(t)] E_b\} \\ &= \exp\left[i\frac{\pi}{V_\pi} \text{data}(t)\right] E_c \end{aligned} \quad (2)$$

which means that the output lightwave signal is modulated by the DPSK and FSK signals.

From (2), one can see that the modulation process is equivalent to that in Fig. 1; two peaks in the spectrum can be clearly seen at the output. Fig. 2(a)–(e) sketches the spectra and illustrates the principle of the FSK modulation. The output of the sub-MZM that is driven by the cosine signal (upper) has two sidebands without phase difference, whereas the one from the other sub-MZM that is driven by the sine signal (lower) shows two sidebands with 180° phase difference relative to each other, and the two sidebands are orthogonal to those of the upper MZM. As the phase modulator C_1 does not provide relative phase shift, the spectrum at point C is the same as that at point A. However, the signal spectrum at the lower path rotates either counterclockwise (for USB) or clockwise (for LSB) at point D. This can ensure that there is no 90° or 180° initial phase difference between the USB and the LSB. After the sum operation of the USB and LSB components, an FSK signal is generated. A pulse carver can be cascaded to obtain return-to-zero (RZ)-DPSK/FSK, as we will use the RZ-DPSK/FSK to analyze the IFWM effects.

B. Label Erasing and the Detecting Scheme

A DSB modulator based on a standard MZM is used to remove the FSK label. It can be the same as the DSB suppressed carrier (SC) in [12], [20], and [21]. To ensure that the two sidebands are in phase, a cosine signal with a frequency equal to the frequency deviation of the FSK signal is needed to drive the MZM, whose transfer function can be expressed as [21]

$$\frac{i}{2} J_1(A'_m) [\exp(i\omega_m t) + \exp(-i\omega_m t)] \quad (3)$$

where A'_m is the amplitude of the clock signal. The higher order Bessel series are neglected. The equation shows that the USB and the LSB of the DSB signal have the same initial phases. Therefore, the main lobe of the output signal after the DSB modulator at the carrier f_0 contains the DPSK phase information without additional impact induced by the FSK label, and the recovered DPSK signal possesses the same phase difference between neighboring pulses as the original DPSK payload.

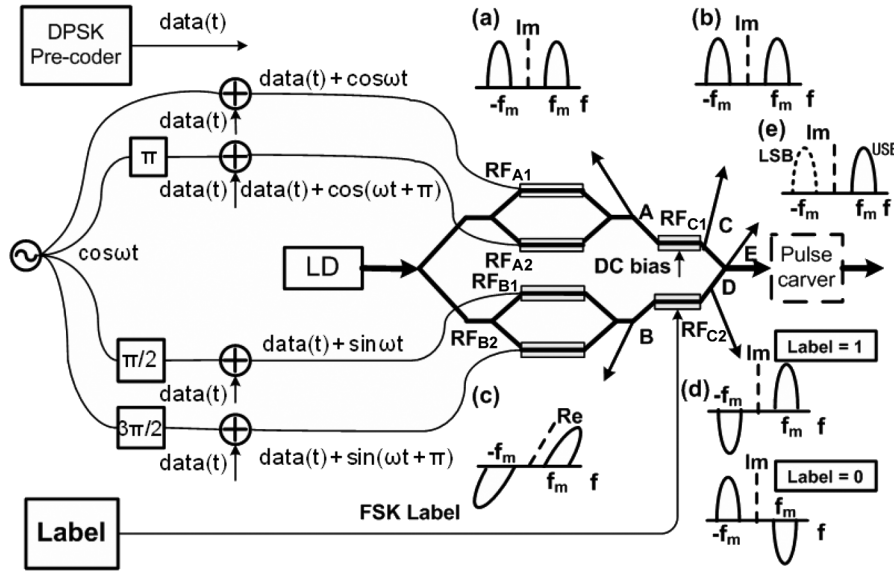


Fig. 2. DPSK/FSK modulation based on a dual-parallel modulator. (a)–(e) Principle of FSK modulation.

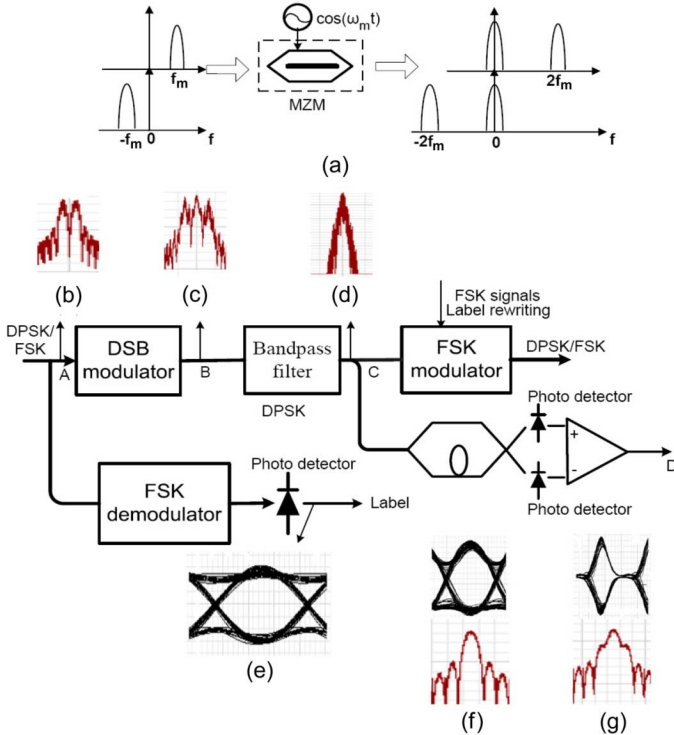


Fig. 3. Label erasing and payload/label detection. (a) Frequency shift process by DSB modulator. Optical spectra (b) before the DSB modulator (point A), (c) after the DSB modulator (point B), and (d) after the bandpass filter (point C). (e) Eye diagram of the FSK label signal. Eye diagrams and spectra of (f) NRZ DPSK payload signal and (g) RZ DPSK payload signal (point D), respectively.

Fig. 3 shows the schematic of label erasing and payload/label detection. Fig. 3(a) illustrates the process of the frequency shift by the DSB modulator. When the FSK label is “1,” the output optical signal has two carrier frequencies of f_0 and $f_0 + 2f_m$, whereas when the FSK label is “0,” the output signal possesses carrier frequencies of f_0 and $f_0 - 2f_m$. Thus, the optical spectrum after the DSB modulator shows three peaks at $f_0 - 2f_m$, f_0 , and $f_0 + 2f_m$, respectively [Fig. 3(c)]. By using a bandpass

filter with a center frequency of f_0 , the DPSK payload signal can be recovered with only one carrier frequency [Fig. 3(d)]. As the phase of the DPSK signal does not affect the frequency deviation of the FSK signal, the FSK label can be detected using a simple demodulation scheme such as with a bandpass filter [12]. The electrical eye diagram of the recovered FSK signal is shown in Fig. 3(e). After erasing the FSK label, one can either add a new FSK label to the payload or demodulate the DPSK signal through a one-bit delay MZI and balanced detectors. The electrical eye diagrams of the recovered nonreturn-to-zero (NRZ)-DPSK and RZ-DPSK signal with a 50% duty cycle are provided in Figs. 3(f) and (g), respectively.

In practice, the imperfections of the modulators are issues of concern in affecting the performance of the DPSK/FSK signal. From the published experimental results, the dual-parallel modulator in [18] has a suppression ratio of 17 dB, and a typical DSB modulator based on a standard MZM shows at least 25-dB carrier-suppression ratio. Thus, the suppression ratio of the largest in-band crosstalk originating from the unsuppressed carrier and the sidebands of the modulator is higher than 42 dB, which would not cause significant impairments [24]. The number of the label rewriting processes may be also limited by the performances of the dual-parallel modulator and the DSB-SC modulator. This problem could be solved as the device performance improves or if a phase-regeneration scheme is employed in label switching systems [25].

III. NONLINEAR PERFORMANCE OF THE DPSK/FSK IN SUPPRESSING THE IFWM

In this section, we investigate the tolerance of the DPSK/FSK to the IFWM, whose impacts to the DPSK and the FSK should be separately treated. However, here, we only study the quality of the recovered DPSK signal through transmission for two reasons: 1) we find out that certain IFWM components of the DPSK/FSK signal after the nonlinear transmission can be filtered; therefore, they do not significantly impair the FSK

label; and 2) the transmission distance of the FSK label signal is typically not long enough to induce significant degradation before the old label is erased and a new label is added; however, the DPSK payload signal will go through a number of network nodes, and the quality of the DPSK signal may be severely degraded by the IFWM. In Section III-A, we derive an expression for the IFWM component of the DPSK/FSK signal and discuss some spectral properties of the IFWM components. In Section III-B, the robustness of the recovered DPSK signal to the IFWM is shown through simulations.

A. Expression of the IFWM Component for the DPSK/FSK and its Spectral Properties

We use a model similar to that in [14] to investigate the IFWM in the hybrid modulation format. In our study, we neglect nonlinear interactions between the signal and the amplified spontaneous emission noise [14]. A single dispersion manage span includes a piece of a dispersion compensation fiber (DCF) for precompensation, a standard single-mode fiber (SSMF) for transmission, and a DCF for postcompensation, where the nonlinearity of the DCF is neglected, and precompensation and postcompensation are exactly one half of the total dispersion of the SSMF. For simplicity, in Section III, we neglect the third and higher order dispersion terms and the fiber loss. In this section, we focus on the nonlinear transmission performance of the DPSK/FSK format and assume an ideal DSB-SC modulation process.

Here, we assume that the RZ-DPSK/FSK signal is a pulse train consisting of a series of Gaussian pulses denoted as $A_l = \sum_k A_k(z, t) = \sum_k A(z, t - kT)$, and the k th pulse before transmission can be expressed as

$$A_k(0, t) = a_k A_0 \exp(-i\Omega_k t) \exp\left[-\frac{(t - kT)^2}{2\tau_0^2}\right] \quad (4)$$

where $a_k = \pm 1$, representing the DPSK information; $\Omega_k = \pm 2\pi f_m$ is the frequency deviation relative to the carrier frequency (in radians per second), representing the FSK information. A_0 is the pulse amplitude, which is equal to $\sqrt{(P_0/\sqrt{\pi}\tau_0 T)}$, where P_0 is the initial injected pulse power, and τ_0 and T are the pulsewidth and the bit period, respectively.

Similar to [22], using the perturbation method, the perturbation term A_p satisfies the following equation:

$$\frac{\partial A_p}{\partial z} + i\frac{\beta_2}{2} \frac{\partial^2 A_p}{\partial t^2} = i\gamma \sum_{l,m,n} A_l A_m \bar{A}_n \quad (5)$$

where β_2 and γ are the group velocity dispersion parameter and the nonlinear coefficient, respectively. This equation contains all the nonlinear effects; the IFWM corresponds to the case when the indexes satisfy $l \neq n$ and $m \neq n$. By taking the Fourier transform and the inverse Fourier transform to solve (5), we obtain a general expression of the IFWM component that is centered at the k th time slot produced by three contributing

pulses located at the l th, m th, and n th time slots [22], respectively, i.e.,

$$\begin{aligned} A_p(L, t) = & ia\gamma A_0^3 \exp[-iT_*(l\Omega_{l,*} + m\Omega_{m,*} - n\Omega_{n,*})] \\ & \times \exp\left[-\frac{1}{2}(\Omega_{l,*}^2 + \Omega_{m,*}^2 + \Omega_{n,*}^2)\right] \exp\left(-\frac{1}{6}t'^2\right) \\ & \times \int_{-\frac{L}{2}}^{\frac{L}{2}} dz \frac{1}{\sqrt{1+2i\beta_*+3\beta_*^2}} \\ & \times \exp\left\{\frac{-3\left[\frac{2t'}{3} + (T_l - \bar{T}_n)\right]\left[\frac{2t'}{3} + (T_m - \bar{T}_n)\right]}{1+3i\beta_*}\right\} \\ & \times \exp\left[-\frac{(T_l - T_m)^2}{(1-i\beta_*)(1+3i\beta_*)}\right] \end{aligned} \quad (6)$$

where $a = a_l a_m a_n$, $\beta_* = \beta_2 z / \tau_0^2$, $t' = t_* - (T_l + T_m - \bar{T}_n)$, $t_* = t / \tau_0$, $T_k = kT_* - i\Omega_{k,*} T_*$, $T_* = T / \tau_0$, and $\Omega_{k,*} = \Omega_k \tau_0$ are all in the normalized forms.

A similar formula for the OOK or (D)PSK signals was presented in [16]. Comparing the above equation with (6), it can be seen that the expression for the OOK or the (D)PSK is a special situation when the frequency deviations are all set to zero. The term $\exp(-(1/6)t'^2)$ can be expanded to

$$\begin{aligned} \exp\left(-\frac{1}{6}t'^2\right) = & \exp\left\{-\frac{1}{6}[t_* - (l + m - n)T_*]^2\right\} \\ & \times \exp\left[\frac{1}{6}(\Omega_{l,*} + \Omega_{m,*} + \Omega_{n,*})^2\right] \\ & \times \exp\left[\frac{1}{3}i(l + m - n)T_*(\Omega_{l,*} + \Omega_{m,*} + \Omega_{n,*})\right] \\ & \times \exp\left[-\frac{1}{3}i(\Omega_{l,*} + \Omega_{m,*} + \Omega_{n,*})t_*\right]. \end{aligned} \quad (7)$$

The first part of the expansion $\exp\{-(1/6)[t_* - (l + m - n)T_*]^2\}$ reveals that for the DPSK/FSK, the shape of the IFWM component is still Gaussian, and the pulsewidth is broadened to $\sqrt{3}$ times of the signal pulse. The central temporal position of the perturbation is located at $t = (l + m - n)T$. The second part of the expansion $\exp[(1/6)(\Omega_{l,*} + \Omega_{m,*} + \Omega_{n,*})^2]$, together with the term $\exp[-(1/2)(\Omega_{l,*}^2 + \Omega_{m,*}^2 + \Omega_{n,*}^2)]$ in (6), is an attenuation term caused by the FSK. The third part, i.e., $\exp[(1/3)i(l + m - n)T_*(\Omega_{l,*} + \Omega_{m,*} + \Omega_{n,*})]$, combined with the term $\exp[-iT_*(l\Omega_{l,*} + m\Omega_{m,*} - n\Omega_{n,*})]$ in (6), is a constant phase shift. The fourth part, i.e., $\exp[-(1/3)i(\Omega_{l,*} + \Omega_{m,*} + \Omega_{n,*})t_*]$, however, is not seen in the expression of the OOK or the DPSK. It shows that unlike the DPSK, the IFWM component has a frequency shift of $(1/3)(\Omega_l + \Omega_m + \Omega_n)$. As $|\Omega_l| = |\Omega_m| = |\Omega_n| = \Omega$, the frequency shift is either $\pm\Omega$ or $\pm(\Omega/3)$.

In the following, we show that this frequency deviation contributes to nearly the total frequency shift of the IFWM component. If the Fourier transform of the IFWM component $A_p(L, \omega)$ can be expressed as a function of the form $f(\omega - \omega_0)$ with its center at $\omega = \omega_0$, ω_0 is then the frequency deviation. Fig. 4(a) shows four typical cases by plotting $|A_p(L, \omega)|$ of several arbitrarily chosen sets of (l, m, n) and $(\Omega_l, \Omega_m, \Omega_n)$. $(1/3)(\Omega_l +$

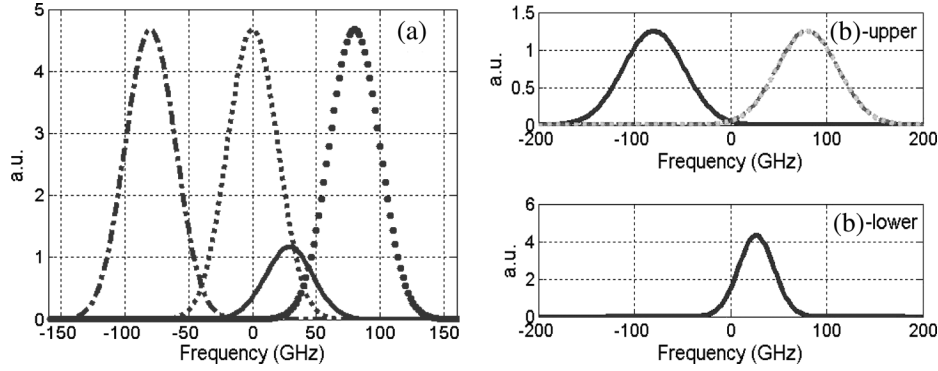


Fig. 4. (a) Perturbations produced by three pulses whose indexes are $(l, m, n) = (1, 5, 2)$, and the corresponding frequency deviations are as follows: (dashed) $f_1 = f_2 = f_3 = 0$; (solid) $f_1 = f_2 = 80$ GHz, $f_3 = -80$ GHz; (circle) $f_1 = f_2 = f_3 = 80$ GHz; (dot-dashed) $f_1 = f_2 = f_3 = -80$ GHz. The x -axis is set relative to the carrier frequency. (b) Upper: spectra of three pulses with frequency deviations of Ω , Ω , and $-\Omega$. Lower: multiplication of the spectra in the upper plot.

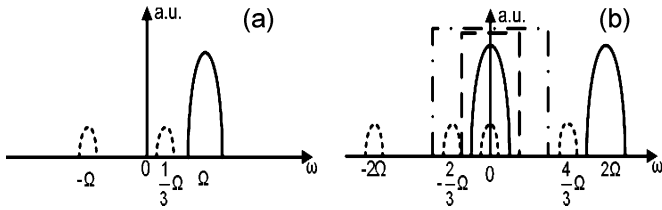


Fig. 5. Spectra of the k th DPSK pulse with the frequency deviation of (solid) Ω and two typical IFWM components located at the k th time slot with frequency deviations of (dashed) $-\Omega$ and $(1/3)\Omega$ (a) before the DSB modulator and (b) after the DSB modulator, respectively. (dashed rectangle) Bandpass filter with bandwidth less than $(4/3)\Omega$. (dot-dashed rectangle) Bandpass filter with bandwidth wider than $(4/3)\Omega$. The x -axis is set relative to the carrier frequency.

$\Omega_m + \Omega_n$) can be a good approximation to the frequency shift of the IFWM component. Note that Fig. 4(a) also reveals that the IFWM component resulting from three pulses with the same frequency deviation shows higher amplitude than that from three pulses having different frequency deviations.

The factor of one third in the IFWM frequency term only holds for Gaussian pulses and does not seem to follow the general FWM process $(\omega + \omega_1) + (\omega + \omega_2) - (\omega + \omega_1 + \omega_2) \rightarrow \omega$, which describes the energy conservation among the four waves involved. Here, we explain the fractional factor from another view in the frequency domain. For a DPSK/FSK pulse train, the IFWM component resulting from three pulses at T_1 , T_2 , and T_3 is approximately proportional to the convolution of three functions $P^{(0)}(t - T_1)$, $P^{(0)}(t - T_2)$, and $P^{(0)*}(-t - T_3)$ [26], where $P^{(0)}(t)$ is the initial shape of a single pulse. For a Gaussian-shaped signal, its spectrum is still Gaussian that is centered at $\omega_0 \pm \Omega$. As the convolution in the time domain corresponds to the multiplication in the frequency domain, it is straightforward to find out that the multiplication of three Gaussian spectra that are centered at Ω_1 , Ω_2 , and Ω_3 leads to a Gaussian spectral component at $(1/3)(\Omega_1 + \Omega_2 + \Omega_3)$. Fig. 4(b) shows a case for three pulses having frequency deviations of Ω , Ω , and $-\Omega$.

B. Performance Evaluations for the DPSK/FSK

Equation (6) is the expression of the IFWM component before label erasing. Here, we evaluate the quality of the demodulated DPSK signal. To recover the DPSK signal, one needs to

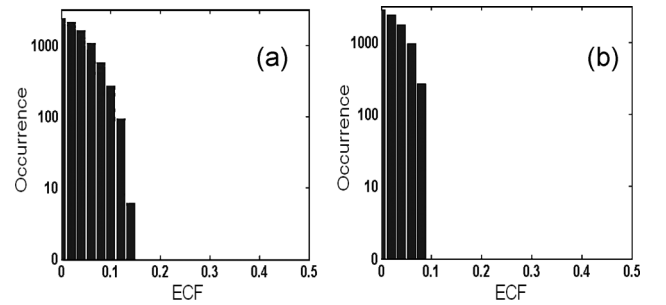


Fig. 6. ECF histograms for (a) recovered DPSK signal from the DPSK/FSK under the assumption that the IFWM components at $\omega_0 \pm (1/3)\Omega$ are totally filtered and (b) recovered DPSK signal from the DPSK/FSK under the assumption that the IFWM components at $\omega_0 \pm (1/3)\Omega$ are completely kept.

erase the FSK signal using a DSB modulator and a bandpass filter, a process in which the IFWM components also experience the frequency shift and the filtering. Here, we assume that the ideal rectangular-shaped bandpass filter is noise free and has a net unit gain.

As discussed in Section III-A, the frequency shift of the IFWM component is either $\pm\Omega$ or $\pm(\Omega/3)$. When it is $\pm\Omega$, the spectra of the IFWM components locate at ω_0 and $\omega_0 \pm 2\Omega$ after the DSB modulator. On the other hand, if the frequency shift of the IFWM component is $\pm(\Omega/3)$, the spectral components of the IFWM after the DSB modulator are at $\omega_0 \pm (2/3)\Omega$ and $\omega_0 \pm (4/3)\Omega$. Fig. 5(a) shows that two IFWM components with frequency deviations of $-\Omega$ and $(1/3)\Omega$ are generated at the location of a DPSK pulse having a frequency deviation of Ω . After the DSB modulator, the pulse is shifted to ω_0 and $\omega_0 + 2\Omega$, whereas the IFWM component originally at $\omega_0 - \Omega$ is moved to ω_0 and $\omega_0 - 2\Omega$, and that at $\omega_0 + (1/3)\Omega$ is shifted to $\omega_0 - (2/3)\Omega$ and $\omega_0 + (4/3)\Omega$. If the bit rate of the DPSK signal is much lower than $(2/3)\Omega$, one can use a bandpass filter that is centered at ω_0 with a bandwidth that is smaller than $(4/3)\Omega$ [Fig. 5(b)] to remove some of the IFWM components, and only the IFWM terms in the DPSK/FSK format with frequency shifts of $\pm\Omega$ remain in the recovered DPSK signal. On the other side, if the bit rate of the DPSK signal is close to Ω , the IFWM component of $(1/3)\Omega$ may remain but to a lesser extent. Here, we assume that the frequency deviation should be

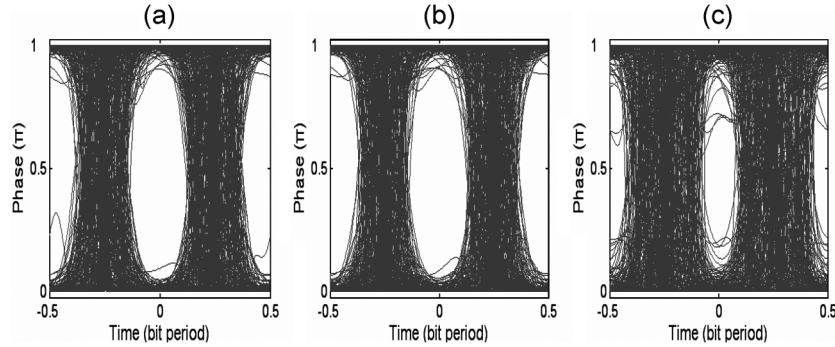


Fig. 7. Differential phase eye diagram of (a) recovered DPSK signal from the DPSK/FSK, (b) conventional DPSK signal, and (c) recovered DPSK signal from the DPSK/ASK with an extinction ratio of 8 dB.

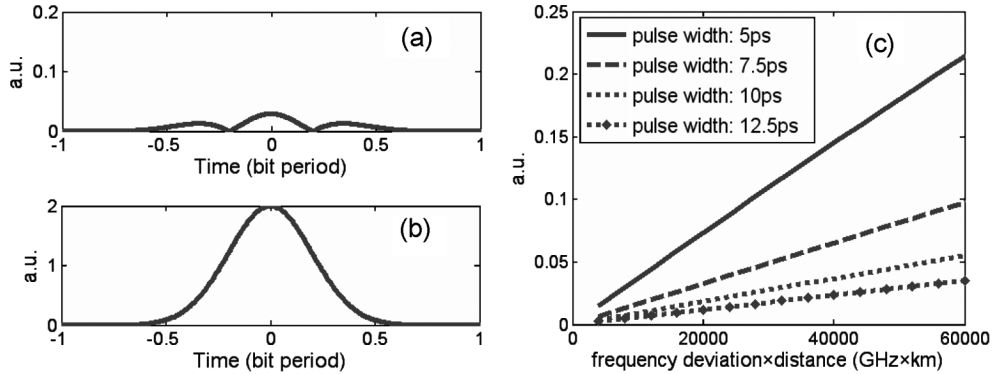


Fig. 8. Differential term after the delay-and-subtraction operation for two neighboring DPSK pulses (a) with the same polarity and opposite frequency deviations and (b) with the opposite polarity and frequency deviations. (c) Normalized peak amplitude of the demodulated signal from two neighboring in-phase DPSK signals versus the product of the distance and the frequency deviation with different pulsewidths.

larger than the bit rate of the DPSK signal to ease the design of the bandpass filter and reduce the crosstalk.

In our simulations, we used a 40-Gb/s DPSK signal having a pulsewidth of 5 ps and a 10-Gb/s FSK label with a frequency deviation of 80 GHz. The carrier wavelength is 1550 nm, the dispersion parameter D of the 100-km SSMF is 17 ps/(nm · km) ($\beta_2 = -22$ ps²/km), the nonlinear coefficient of the transmission fiber is $\gamma = 1.2$ rad/(W · km), and the DCF has a dispersion parameter $D = -100$ ps/(nm · km).

Here, we use the eye closure factor (ECF) similar to that in [14] and [15] to evaluate the performance of the recovered DPSK signal. The pattern length that is required in a simulation is described as follows [27]:

$$m \geq CD_{\max} \lambda^2 B \frac{\Delta f}{c} + 1 \quad (8)$$

where CD_{\max} is the maximum accumulated dispersion, λ is the wavelength of the carrier, B is the bit rate of the DPSK signal, Δf is the bandwidth of the DPSK signal, and c is the speed of light. Substituting the corresponding parameters into (8) leads to $m \geq 14$. Consider a sequence consisting of 14 bits. Through calculating $\Delta\phi_7$ and $\Delta\phi_8$, one can get the ECF of the center bit. Assuming that $a_1 = 1$, we exhaust all $2^{13} = 8192$ polarity combinations for the remaining 13 pulses. Here, we consider two extreme cases: the IFWM components at $\omega_0 \pm (1/3)\Omega$ are totally filtered, whereas in the other case, the IFWM components at $\omega_0 \pm (1/3)\Omega$ all remain. Figs. 6(a) and (b) shows

the histograms of the ECFs of the recovered DPSK signal from the DPSK/FSK format under these two assumptions, respectively. The average launch power is set to 8.5 dBm to observe the eye closure. The ECF is smaller under the assumption that the IFWM components are all kept. This is mainly due to the fact that the DPSK is a bipolar signal. The FSK signal can change the instantaneous phase of the DPSK signal and, thus, vary the polarity distribution of the DPSK; therefore, the IFWM components at $\omega_0 \pm (1/3)\Omega$ can cancel those at $\omega_0 \pm \Omega$ to some extent, although the amplitudes of the IFWM components at $\omega_0 \pm (1/3)\Omega$ are much smaller than those at $\omega_0 \pm \Omega$. In practice, the IFWM components at $\omega_0 \pm (1/3)\Omega$ cannot be completely filtered nor totally kept. Both the filtering and the cancellation effects may be present; the ECF could be between the two extreme cases.

To further investigate the transmission performance of the DPSK/FSK format, we use a pseudorandom bit sequence of length $2^9 - 1$ to plot the eye diagram of the differential phase of the recovered DPSK to compare it with a conventional DPSK signal [Fig. 7(a) and (b)]. The simulation parameters are the same as those used in the analysis except that the average launch power is increased to 15 dBm to induce evident penalties, and the effects of self-phase modulation and cross-phase modulation are included. The bandwidth of the bandpass filter that is used to recover the DPSK signals from the DPSK/FSK is 160 GHz. It shows that the recovered DPSK signal possesses nearly the same eye opening compared to that of the conventional DPSK signal.

On the other hand, we provide the eye diagram of a recovered DPSK signal from a DPSK/ASK signal with an extinction ratio of 8 dB under the same average launch power. Fig. 7(c) clearly shows the improvement of the FSK-labeled DPSK compared with the ASK-labeled DPSK to combat nonlinear impairments. Note that this phase impairment is in addition to the penalty that is caused by the ASK modulation, which is not seen in the DPSK/FSK format.

In practice, fiber loss should be taken into account, and the IFWM effect is weaker as the IFWM-induced amplitude fluctuation is proportional to the effective length of the fiber. The optimal dispersion precompensation for the single-span model used in our simulation should be less than half of the total cumulated dispersion, as the power profile is no longer symmetric with respect to the center of the fiber when considering the fiber loss [16], [26]. However, most practical transmission systems consist of multiple spans, and each span has inline dispersion compensation and amplification. As discussed in [26], the simple single-span model neglecting the fiber loss with symmetric dispersion compensation is a good approximation for characterizing the property of a practical multiple-span transmission system. Thus, our IFWM analysis using this simple model is an approximation to the practical multiple-span systems.

IV. DISPERSION SLOPE TOLERANCE OF THE DPSK/FSK

In a real system, tunable dispersion compensation is employed to accurately compensate the accumulated dispersion at the receiver site. However, dispersion cannot be completely compensated over a frequency band due to the dispersion slope S (or third-order dispersion parameter β_3) of the transmission fiber. The dispersion slope should be taken into account [28], particularly for the DPSK/FSK whose bandwidth is wider than other nonhybrid formats. Here, we consider a simple model to investigate the impact of the dispersion slope. Assume that the dispersion is completely compensated at the carrier frequency of the DPSK signal. Then, there exists small residual dispersion at $\omega_0 \pm \Omega$. We consider two pulses with frequency deviations of $\pm\Omega$; thus, they have the same group velocity, and there is no walk-off between the two pulses. However, there may be additional phase difference between two neighboring pulses with different frequency deviations, as the residual dispersions at $\omega_0 \pm \Omega$ are opposite. This may cause some penalty since the correct demodulation of the DPSK signal depends on the phase difference between the neighboring pulses.

With the Gaussian pulse train used in Section III, Fig. 8 shows the results of one-bit delay and subtraction of two neighboring DPSK bits with different FSK labels; the dispersion parameter S_{SMF} is 0.06 ps/(nm · km), and $S_{\text{DCF}} = -0.67$ ps/(nm · km). Other parameters are the same as those in Section III. Fig. 8 shows that when the neighboring DPSK signals are in phase, the differential term of the DPSK signal after the delay-and-subtraction operation exhibits a small peak at the center of the pulse, causing the eye closure penalty. As the residual dispersion is proportional to the transmission distance and the frequency deviation, this term should be also proportional to the product of the distance and the frequency deviation. Fig. 8(c) shows the

amplitude of such a small peak component at the center of the pulse versus the product of the distance and the frequency deviation with different pulsewidths for the 40-Gb/s DPSK signals. In general, the dispersion-slope-induced penalty is not expected to be severe within reasonable transmission distances (e.g., <1000 km) and frequency deviations for the FSK label (e.g., 80 GHz in this study).

V. CONCLUSION

We have presented a new modulation scheme using a dual-parallel modulator to generate the DPSK/FSK signal. We have also proposed a method for label erasing and payload detection based on a DSB modulator and an MZI.

In Section III, we have derived the IFWM term of the hybrid modulation format when neglecting the dispersion slope. We have verified that this IFWM component has a frequency deviation that is one third of the sum of the frequency deviations of the three interacting pulses that are contributing to the IFWM under the assumption that the pulses are Gaussian shaped. We have evaluated the nonlinear performance of the DPSK payload signal using the ECF and provided the eye diagram of the recovered DPSK signal and compared it with that of the conventional DPSK and the recovered DPSK payload from a DPSK/ASK data signal. The results showed that the demodulated DPSK payload presents similar performance to the conventional DPSK signal without labeling and clearly outperforms the DPSK payload from a DPSK/ASK format.

In Section IV, we have discussed the tolerance of the DPSK/FSK format to the dispersion slope of the transmission fiber. We have shown that the dispersion slope induces negligible penalty within reasonable transmission distances.

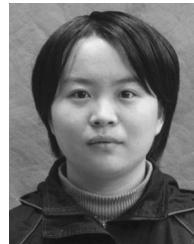
ACKNOWLEDGMENT

The authors would like to thank P. Voss and C. Xie for their helpful comments and insightful discussions.

REFERENCES

- [1] S. Yoo, "Optical-packet switching and optical-label switching technologies for the next generation optical Internet," in *Proc. OFC*, Atlanta, GA, 2003, pp. 797–798, Paper FS5.
- [2] D. J. Blumental, B. E. Olsson, G. Rossi, T. E. Dimmick, L. Raul, M. Masanovic, O. Lavrova, R. Doshi, O. Jerphagnon, J. E. Bowers, V. Kaman, L. A. Coldren, and J. Barton, "All optical label swapping networks and technologies," *J. Lightw. Technol.*, vol. 18, no. 12, pp. 2058–2075, Dec. 2000.
- [3] J. Yu and G.-K. Chang, "A novel technique for optical label and payload generation and multiplexing using optical carrier suppression and separation," *IEEE Photon. Technol. Lett.*, vol. 16, no. 1, pp. 320–322, Jan. 2004.
- [4] T. Koonen, G. Mothier, J. Jennen, H. Waardt, and P. Demeester, "Optical packet routing IP-over-WDM networks deploying two-level optical labeling," in *Proc. ECOC*, Amsterdam, The Netherlands, 2001, pp. 14–15.
- [5] N. Chi, B. Carlsson, P. V. Holm-Nielsen, C. Peucheret, and P. Jeppesen, "Dispersion management for two-level optically labeled signals in IP-over-WDM networks," in *Proc. ECOC*, Copenhagen, Denmark, 2002, pp. 1–2, Paper 5.5.1.
- [6] T. Koonen, S. Silur, I. Monroy, J. Jennen, and H. Waardt, "Optical labeling of packets in IP-over-WDM networks," in *Proc. ECOC*, Copenhagen, Denmark, 2002, pp. 1–2, Paper 5.5.2.
- [7] N. Chi, J. Zhang, P. V. Holm-Nielsen, C. Peucheret, and P. Jeppesen, "Transmission and transparent wavelength conversion of an optical labeled signal using ASK/DPSK orthogonal modulation," *IEEE Photon. Technol. Lett.*, vol. 15, no. 5, pp. 760–762, May 2003.

- [8] X. Liu, X. Wei, Y. Su, J. Leuthold, Y.-H. Kao, I. Kang, and R. C. Giles, "Transmission of an ASK-labeled RZ-DPSK signal and label erasure using a saturated SOA," *IEEE Photon. Technol. Lett.*, vol. 16, no. 6, pp. 1594–1596, Jun. 2004.
- [9] X. Liu, Y. Su, X. Wei, J. Leuthold, and R. C. Giles, "Optical-labeling switching based on DPSK/ASK modulation format with balanced detection for DPSK payload," presented at the Eur. Conf. Optical Commun. (ECOC), Rimini, Italy, 2003, Paper Tu4.4.3.
- [10] N. Chi, C. Milkkelsen, L. Xu, J. Zhang, P. V. Holm-Nielsen, H. Ou, J. Seonae, C. Peucheret, and P. Jeppesen, "Transmission and label encoding/erasure of orthogonally labeled signal using 40 Gb/s RZ-DPSK payload and 2.5 Gb/s IM label," *Electron. Lett.*, vol. 39, no. 18, pp. 1335–1337, Sep. 2003.
- [11] W.-R. Peng, Y.-C. Lu, J.-H. Chen, and S. Chi, "ASK/RZ-DPSK labelled signal generation using only one Mach-Zehnder modulator," presented at the Eur. Conf. Optical Commun. (ECOC), Cannes, France, 2006, Paper Mo4.4.6.
- [12] T. Kawanishi, K. Higuma, T. Fujita, J. Ichikawa, T. Sakamoto, S. Shinada, and M. Izutsu, "High-speed optical FSK modulator for optical packet labeling," *J. Lightw. Technol.*, vol. 23, no. 1, pp. 87–94, Jan. 2005.
- [13] J. Vegas Olmos, I. Monroy, A. Koonen, and Y. Yu, "High bit-rate combined FSK/IM modulated optical signal generation by using GCSR tunable laser sources," *Opt. Express*, vol. 11, no. 23, pp. 3136–3140, 2003.
- [14] X. Wei and X. Liu, "Analysis of intrachannel four-wave mixing in differential phase-shift keying transmission with large dispersion," *Opt. Lett.*, vol. 28, no. 23, pp. 2300–2302, 2003.
- [15] R. J. Essiambre, B. Mikkelsen, and G. Raybon, "Intra channel cross-phase modulation and four-wave mixing in high-speed TDM systems," *Electron. Lett.*, vol. 35, no. 18, pp. 1576–1578, Sep. 1999.
- [16] A. Mecozzi, C. B. Clausen, and M. Shtaif, "Cancellation of timing and amplitude jitter in symmetric links using highly dispersed pulses," *IEEE Photon. Technol. Lett.*, vol. 13, no. 5, pp. 445–447, May 2001.
- [17] F. Zhang, C. A. Bunge, K. Petermann, and A. Richter, "Optimal dispersion mapping of single-channel 40 Gb/s return-to-zero differential phase-shift keying transmission systems," *Opt. Express*, vol. 14, no. 15, pp. 6613–6618, Jul. 2006.
- [18] T. Kawanishi, K. Higuma, T. Fujita, S. Mori, S. Oikawa, J. Ichikawa, T. Sakamoto, and M. Izutsu, "40 Gb/s versatile LiNbO₃ lightwave modulator," presented at the Eur. Conf. Optical Commun. (ECOC), Glasgow, U.K., 2005, Paper Th2.2.6.
- [19] T. Kawanishi, M. Izutsu, T. Sakamoto, and T. Miyazaki, "High speed DQPSK and FSK modulation using integrated Mach-Zehnder interferometers," *Opt. Express*, vol. 14, no. 10, pp. 4469–4478, May 2006.
- [20] T. Kawanishi, T. Sakamoto, M. Tsuchiya, and M. Izutsu, "70 dB extinction-ratio LiNbO₃ optical intensity modulator for two-tone lightwave generation," presented at the Opt. Fiber Commun. (OFC), Anaheim, CA, 2005, Paper OWC4.
- [21] T. Kawanishi, M. Izutsu, and T. Sakamoto, "All optical modulation format conversion from frequency-shift-keying to phase-shift-keying by using double sideband modulation technique," presented at the Conf. Lasers Electro-Optics (CLEO), San Francisco, CA, 2004, Paper CW01.
- [22] J. Zweck and C. R. Menyuk, "Analysis of four-wave mixing between pulses in high-data-rate quasi-linear subchannel-multiplexed systems," *Opt. Lett.*, vol. 27, no. 14, pp. 1235–1237, Jul. 15, 2002.
- [23] S. Shinotsu, S. Oikawa, T. Saitou, N. Mitsugi, K. Kubodera, T. Kawanishi, and M. Izutsu, "LiNbO₃ optical side-band modulator," presented at the Opt. Fiber Commun. (OFC), Baltimore, MD, 2000, Paper PD-16.
- [24] H. K. Kim and S. Chandrasekhar, "Dependence of the in-band crosstalk penalty on the signal quality in optical network systems," *IEEE Photon. Technol. Lett.*, vol. 12, no. 9, pp. 1273–1274, Sep. 2000.
- [25] K. Croussore, I. Kim, C. Kim, Y. Han, and G. Li, "Phase-and-amplitude regeneration of differential phase-shift keyed signals using a phase-sensitive amplifier," *Opt. Express*, vol. 14, no. 6, pp. 2085–2094, Mar. 2006.
- [26] X. Wei, "Power-weighted dispersion distribution function for characterizing nonlinear properties of long-haul optical transmission links," *Opt. Lett.*, vol. 31, no. 17, pp. 2544–2546, Sep. 1, 2006.
- [27] L. K. Wickham, R. J. Essiambre, A. H. Gnauck, P. J. Winzer, and A. R. Chraplyvy, "Bit pattern length dependence of intrachannel nonlinearities in pseudolinear transmission," *IEEE Photon. Technol. Lett.*, vol. 16, no. 6, pp. 1591–1593, Jun. 2004.
- [28] G. P. Agrawal, *Nonlinear Fiber Optics & Applications of Nonlinear Fiber Optics*. New York: Academic, 2001, ch. 3.



Contest in China in 2005.



Fangfei Liu (S'07) received the B.S. degree in electrical engineering from Shanghai Jiao Tong University, Shanghai, China, in 2007.

She is a Research Assistant with the Department of Electronic Engineering, Shanghai Jiao Tong University. Her research interests include advanced modulation formats for high-speed optical communication systems, nonlinear optics in waveguides and fibers, and optical signal processing. In 2007 her work on 160-Gb/s slow light was published in OFC.

Ms. Liu won the National Mathematical Modeling

Yikai Su (M'01–SM'07) received the B.S. degree from Hefei University of Technology, Hefei, China, in 1991, the M.S. degree from Beijing University of Aeronautics and Astronautics, Beijing, China, in 1994, and the Ph.D. degree in electrical engineering from the Northwestern University, Evanston, IL, in 2001.

He was with Crawford Hill Laboratory of Bell Laboratories for three years before joining Shanghai Jiao Tong University, Shanghai, China, as a Full Professor in 2004. He became the Associate Department

Chair of the Department of Electronic Engineering in 2006. He has over 100 publications in prestigious international journals and conferences, including 30+ IEEE PHOTONICS TECHNOLOGY LETTERS papers, more than 20 invited conference presentations, and 8 postdeadline papers. He is the holder of three US patents, with over ten US or Chinese patents pending. His research areas cover ultrahigh-speed transmission and modulation formats, optical signal processing, and enabling devices and modules for new network architectures.

Prof. Su is a Member of OSA. He serves as a Guest Editor of IEEE JOURNAL OF SELECTED TOPICS IN QUANTUM ELECTRONICS. He is the Co-Chair of the Workshop on Optical Transmission and Equalization (WOTE) 2005, ChinaCom2007 Symposium, IEEE/OSA AOE 2007 Slow Light Workshop, Asia Pacific Optical Communications (APOC) 2008 SC3, and a Technical Committee Member of Opto-Electronics and Communications Conference 2008, the Conference on Laser and Electro-Optics Pacific Rim 2007, IEEE LASERS AND ELECTRO-OPTICS SOCIETY (LEOS) summer topical meeting 2007 on ultrahigh-speed transmission, IEEE LEOS 2005–2007, BroadNet2006, the Asia-Pacific Optical Communications Conference 2005, and the International Conference on Optical Communications and Networks 2004. He is a Reviewer of a large number of IEEE and Optical Society of America journals.